Light Scattering by Shear-Induced Defects of Nematic Liquid Crystalline Polymers

S. A. Patlazhan,† J. B. Riti, and P. Navard*

Ecole des Mines de Paris, URA CNRS 1374, B.P. 207, F-06904 Sophia-Antipolis Cedex, France

Received October 24, 1994; Revised Manuscript Received December 8, 1995[⊗]

ABSTRACT: The depolarized light scattering patterns observed at low shear rates for lyotropic and thermotropic nematic main-chain liquid crystalline polymers show very similar aspects. They are composed of two main parts, a long streak perpendicular to the flow direction, with a strong intensity modulation, and four asymmetric lobes. These general features suggest a common origin for this pattern. A simplified model of the defects created in the low shear rate region of a thermotropic polymer (De'Nève, T.; Navard, P.; Kléman, M. *Macromolecules* **1995**, *28*, 1541), was used as the basic scattering unit. It consists of a twist loop, fluctuating around the shearing plane, with a director varying from the flow direction to the vorticity axis. The light scattering by a collection of such objects is theoretically calculated and compared to the experimental behavior of the vertical streak.

1. Introduction

The understanding of the rheology of main-chain nematic polymers has progressed enormously these past 10 years. On the theoretical side, major advances have been obtained through the use of the molecular modeling of rigid rod monodomain nematic polymers[1−4] and attempts[5] have been made to take into account the polydomain nature of the real fluids. It is now well established that there is a sequence of different director behaviors in a simple shear flow going from low to high shear rates. For a monodomain polymer nematic fluid, the director tumbles at low shear rates and is flow aligned at high shear rates. For a real polydomain fluid at low shear rates, the dynamics is averaged over the domain orientation distribution function.[5] Most of the predictions of this model have been favorably compared with experiments.[6,7]

On the experimental side, many results have been obtained from rheological techniques[8−12] and from various rheo-optical methods.[6,7,13−19] Most of the results show that there are two basic flow behaviors in shear, depending on the shear rates. At low shear rates the characteristic features of the tumbling regime are observed, with very long transients, a low order parameter and the presence of many defects. At high shear rates the order parameter is higher, and no defects are visible. At present the theoretical and experimental interpretations are in general qualitative agreement, even if many of the specific details remain unsolved and important differences between different materials are unaccounted for (for example between hydroxypropylcellulose and polypeptide solutions).

There is nevertheless a very important area that is still obscure. It concerns the real nematic organization in the low shear rate region. Apart from specially prepared monodomain nematic fluid,[20,21] the texture of nematic polymers is complex, with a strong spatial variation of the director. This is referred to as the domain structure. It must be said that this is a rather vague term which hides our lack of knowledge of the nature and organization of the defects which are present during flow. The defect texture is clearly apparent when the fluid is sheared and observed with an optical microscope.[22,23] Unfortunately, it is difficult, if not impossible, to study the defects during flow by this method. Most of the time, they are too numerous. One method used recently was to very rapidly cool a sheared thermotropic polymer in order to freeze its flow-induced structure.[24,25] This proved to be instructive since very clear defects were evident at low shear rates, corresponding to the tumbling region. They consist of half-strength disclination loops lying in the shearing plane (defined as containing the flow direction and the gradient direction, respectively, called the x_3 and x_1 axes in the following parts), forming the boundary between a region inside the loop where the director is oriented along the flow direction, and a region outside the loop where the director is oriented along the vorticity axis (called x_2). This model forms the basis of the present work.

Light optical microscopy does not allow a proper determination of the texture during flow. Small angle light scattering is a more powerful tool and it is relatively easy to perform with flowing nematic polymers. All the reported experiments have been performed by probing the x_2-x_3 plane. The results at low shear rates obtained from lyotropic and thermotropic[16,18,23,26] polymers show that the light scattering patterns have common characteristics. Under crossed polarization, called HV (polarization direction H being along the flow direction (x_3)), the scattering pattern consists of a bright streak along the vorticity axis (x_2) and four lobes. Under parallel polarization, called VV and HH, the scattering pattern has also a bright streak along the vorticity axis (x_2) with an elongated halo. A description of these patterns will be given in the Experimental Part of this paper. The common aspect of the small angle light scattering patterns suggests a similar nature of the scattering objects. The characteristic HV pattern shows that these scattering objects have a strong orientation fluctuation character. A four-lobe HV pattern has also been seen at rest when defects are observed by optical microscopy.[27−29] An interpretation considering the director orientation around a collection of half-strength disclinations has been published.[30]

† Permanent address: Institute of Chemical Physics of Russian Academy of Sciences, Chernogolovka, Moscow Region 142432, Russia.

[⊗] Abstract published in *Advance ACS Abstracts,* February 1, 1996.

0024-9297/96/2229-2029$12.00/0

The present work will be based on the observations given in refs 24 and 25. We will consider that during a low shear rate flow, a typical defect loop is created in lyotropic and thermotropic polymers. We will calculate the scattering pattern of one isolated loop and then of a collection of loops. Measurable parameters will be extracted and compared with experiments, concentrating on the behavior of the vertical bright streak. Preliminary results have been given in ref 31. The origin of the four lobes will be briefly addressed in Part 3 of the paper.

The present paper has the following contents. Parts 2 and 3 are a description of the rheo-optical equipment used to study sheared nematic polymers and of the experimental light scattering results for two lyotropic solutions. Optical microscopy results will also be recalled. Part 4 gives the description of the model of the disclination loop that will be proposed as the source of light scattering. Part 5 is the theoretical section. The comparison between the experimental and theoretical results is given in part 6.

2. Experimental Part

2.1. Notations. See the list at the end of the paper.

2.2. Materials and Methods. Experiments were carried out on two lyotropic LCP's. The first was an aqueous solution of hydroxypropylcellulose (HPC Klucel L M_w 100 000) containing 50% w polymer. The second was a 25% solution of poly(benzyl glutamate) (PBG) in *m*-cresol. The procedures used to prepare these solutions are described in ref 16. These two lyotropic solutions are anisotropic. HPC 50% in water forms a cholesteric phase at rest while the PBG 25% in *m*-cresol is nematic. Under a weak flow, these solutions are transformed into a polydomain nematic fluid.[14]

SALS measurements were performed with the constant shear rate rheo-optical system (Instron 3250) which is described in ref 26. The usual metallic parts have been replaced by a transparent cone and a plate cell. The incident beam $\mathbf{s}_0$ is produced by a HeNe laser (λ = 632.8 nm) which passes through the sample parallel to the gradient direction of the shear flow. The sample thickness at the point where the light is incident was about 400 μm.

The direction of the scattered radiation is defined by θ (or $\mathbf{q}$) and μ which are the scattering angle (or scattering vector $\mathbf{q}$ with $q = (4\pi/\lambda)\sin(\theta/2)$) and the azimuthal angle, respectively. The direction of the optical axis of the polarizer with respect to the flow direction is defined by the angle ψ. The optical axis of the analyzer is either parallel or perpendicular to the optical axis of the polarizer. The gradient, vorticity, and flow directions are named x_1, x_2, and x_3 (see Figure 1), respectively.

SALS patterns are observed in a plane (x_2−x_3 plane) perpendicular to the incident beam. They are recorded at a rate of 25 frames/s with a video recorder and digitized into a 512 × 512 pixel matrix with 256 gray levels. These gray levels give semiquantitative information about the scattered intensity.

All the experiments were performed at room temperature (21−22 °C) between crossed polarizers. A more complete description of the experiments and the results will be published later. The evolution of the intensity of the vertical streak (the intensity at the azimuthal angle μ = 90°) was measured for different values of the angle ψ. In order to cancel the influence of the fluctuation of the incident intensity with the different positions of the polarizers, the measured scattered intensity was normalized with respect to the incident intensity for each value of ψ. These measurements were performed for different shear rates ranging from 0.1 to 5 s^{-1} for HPC solution and from 0.5 to 20 s^{-1} for PBG.

3. Experimental Results

3.1. Small Angle Light Scattering Results. As mentioned in the Introduction, SALS patterns observed from lyotropic and thermotropic polymers have the same main features. Ernst et al.[16,23] performed microscopy observations and SALS measurements during flow on two lyotropic solutions: A 60% HPC Klucel E (M_w = 60 000) solution in water and PBLG in *m*-cresol with a PBLG concentration of 19.3%. They observed three different steady state scattering patterns depending on the applied shear rate. An elliptical pattern was observed at very low shear rates, between crossed polarizers. At shear rates higher than a critical shear rate $\dot{\gamma}_c$ it changed into a pattern composed of a bright streak along the x_3 direction and four lobes at about 45° to the polarizer axes. At very large shear rates, the SALS patterns did not show any scattering features, perhaps a weak effect at extremely low scattering angles. Similar results were observed for a cellulosic thermotropic polymer.[32]

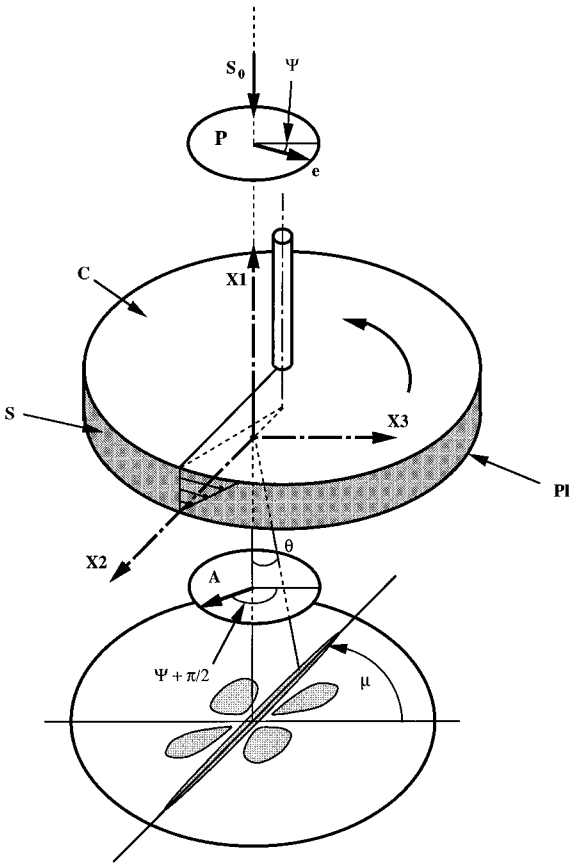

Figure 1. Optical system and the reference coordinate frame: (C) upper cone; (PL) lower plate; (S) sample; (A) analyzer; (P) polarizer; (x_1) shear rate gradient direction; (x_2) vorticity direction; (x_3) flow direction; (θ) scattering angle; (μ) azimuthal angle; (ψ) angle between polarizer direction and flow direction.

For 50% HPC L in water, the transition between the first and the second regions occurred when $\dot{\gamma}$ was between 0.03 and 0.05 s^{-1} ($\dot{\gamma}_c \approx 0.04$ s^{-1}), and for the PBG in *m*-cresol solution, $\dot{\gamma}_c$ was between 0.1 and 0.5 s^{-1}. Typical examples of such SALS patterns are shown in Figure 2. Pictures (a)−(c) show the HV, VV, and HH patterns, respectively, for the 50% hydroxypropylcellulose (HPC Klucel L M_w 100 000) solution at a steady state shear rate of 0.25 s^{-1}. The vertical streak observed in these three cases is mainly due to orientation fluctuations. A quantitative observation showed that the intensity of this vertical streak was more intense for the HV pattern than for the HH pattern which was more intense than for the VV pattern.

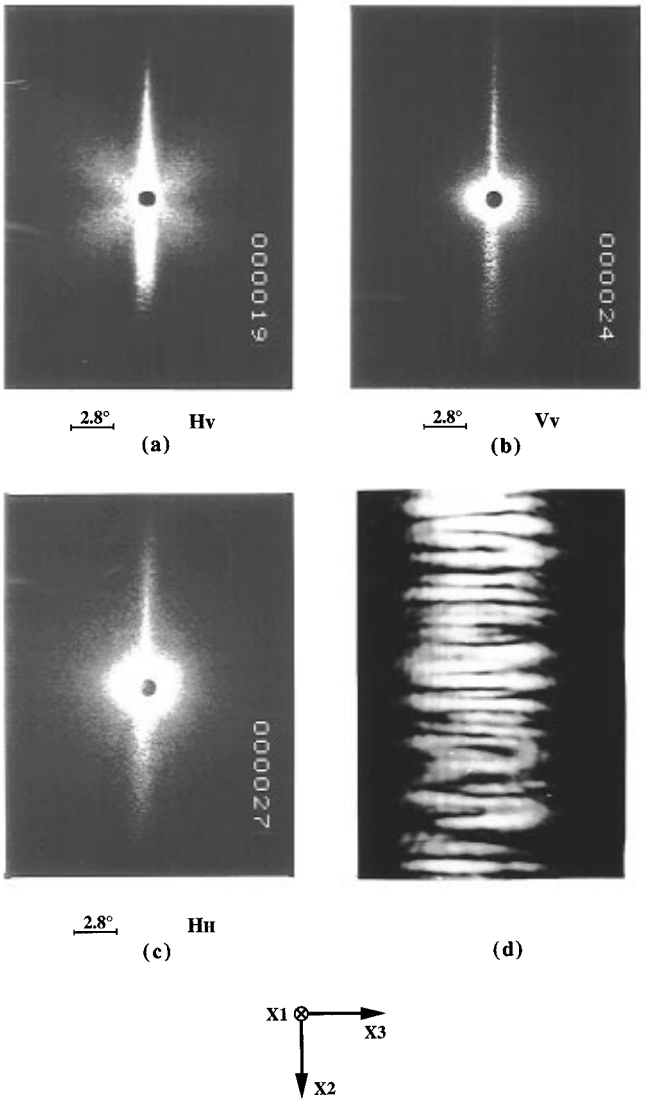

Figure 2. SALS patterns of a 50% HPC L/water solution during a steady state constant shear flow at 0.25 s^{-1}: (a) HV pattern; (b) VV pattern; (c) HH pattern; (d) detail of the vertical streak of the HV pattern; (x_1) gradient direction; (x_2) vorticity axis; (x_3) flow direction.

Picture (d) of Figure 2 is a close-up of the vertical streak of the HV pattern. We can clearly observe that this vertical streak is composed of a set of small intense lines perpendicular to the main direction of the streak. The intensity profiles along the 90° azimuthal (angle μ) direction, i.e. along the streak, shown in Figure 3 confirm this observation. The intensity decreases with increasing scattering angle θ from 0.3 to 5°, with pronounced oscillations. The period of these oscillations was not found to depend on the shear rate.

The observation of SALS patterns at different inclinations of the crossed polarizers to the flow direction (angle ψ) showed that the streak is present independent of ψ. In order to measure the evolution of the intensity I of the streak as a function of ψ we calculated the ratio $I(\psi)/I(\psi{=}45)$ at the azimuthal angle $\mu = 90°$, where $I(\psi)$ is the averaged intensity for a scattering angle θ between 2.8 and 3.2°, with the polarizers oriented at the angle ψ. The choice of this θ range is linked to a theoretical interpretation detailed later, but all θ ranges gave the same result. Figures 4 and 5 show $I(\psi)/I(\psi{=}45)$ as a function of ψ for the PBG and the HPC solutions. In both cases, we observed a minimum value for the ratio $I(\psi)/I(45)$ at around $\psi = 45°$. Parts a and b of Figure 6

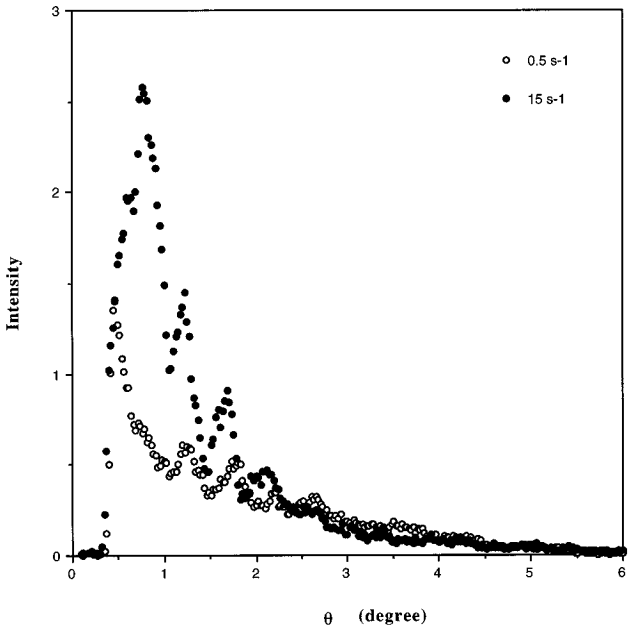

Figure 3. Evolution of the intensity at the azimuthal angle $\mu = 90°$ as a function of the scattering angle θ. PBG 25% *m*-cresol 75% solution for two shear rates, (○) 0.5 s^{-1} and (●) 15 s^{-1}.

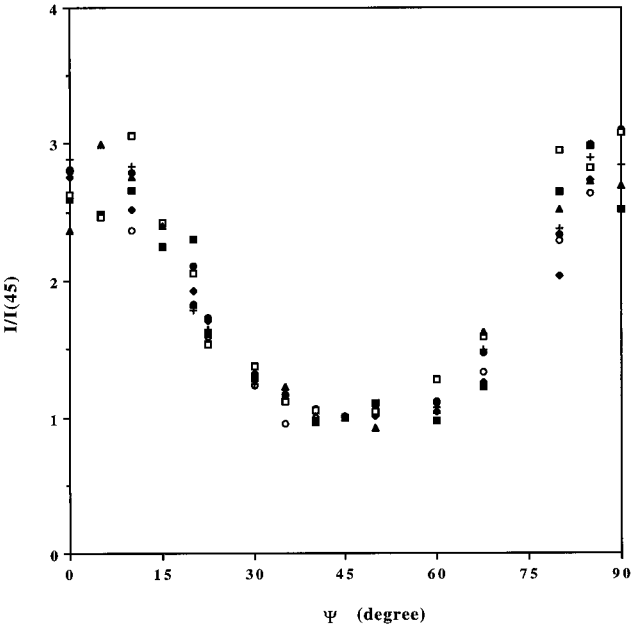

Figure 4. Evolution of the reduced intensity $I/I(45°)$ at $\mu = 90°$ and $\theta = 2.8{-}3.2°$ as a function of the position ψ of the crossed polarizers for different shear rates. PBG 25%−*m*-cresol 75% solution. Key: 0.5 s^{-1} (○); 1 s^{-1} (●); 2.5 s^{-1} (+); 5 s^{-1} (◆); 10 s^{-1} (■); 15 s^{-1} (□); 20 s^{-1} (▲).

give the evolution of $I(0)/I(45)$ as a function of the shear rate. There is a ±10% error for each measurement. For the PBG solution, $I(0)/I(45)$ did not depend on the shear rate (or is slightly decreasing) while it is decreased with increasing shear rate for the HPC solution between 0.2 and 3−4 s^{-1}.

3.2. Observations by Optical Microscopy. Observations by optical microscopy on solutions of PBG and HPC at steady state shear flow and immediately after cessation of flow have been described in the literature.[12,26] at a very small shear rate ($\dot{\gamma} = 0.01$ s^{-1} for HPC and $\dot{\gamma} = 0.05$ s^{-1} for PBG) only a small deformation of the initial texture occurs with a small deformation in the direction of flow. Above a certain

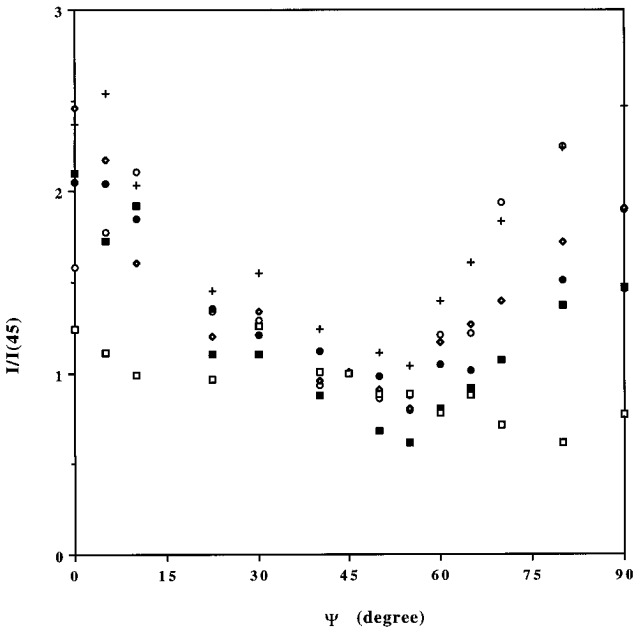

Figure 5. Evolution of the reduced intensity $I/I(45°)$ at $\mu = 90°$ and $\theta = 2.8-3.2°$ as a function of the position ψ of the crossed polarizers for different shear rates. HPC L 50%−water 50% solution. Key: 0.1 s^{-1} (○); 0.25 s^{-1} (●); 0.5 s^{-1} (+); 1 s^{-1} (◆); 2.5 s^{-1} (■); 5 s^{-1} (□).

shear rate ($\dot{\gamma} = 0.1$ s^{-1} for HPC and $\dot{\gamma} = 2.5$ s^{-1} for PBG) a new morphology arises, characterized by the appearance of lines running along the flow direction. Increasing the shear rate makes these lines narrower until they disappear at high shear rates. This corresponds roughly to the three regimes that are seen by light scattering.

After an instantaneous cessation of shear, the light scattering pattern does not change for a few seconds. During this time, the polymer can be observed with an optical microscope, giving an image which reflects the situation just before stopping the flow. It is then possible to see a new structural feature, a set of small dark spots, that was not apparent during flow due to movement of the fluid. They were more easily seen for PBG solutions than for HPC and were clearly observed with a thermotropic polymer.[32] As will be seen elsewhere,[32] the lines running parallel to the flow direction can be associated with the vertical streak seen by light scattering while the dark spots are associated with the four lobes.

4. Model of the Defect Structure under Shear Flow

The disclination loops found in a thermotropic polymer and described in refs 24 and 25 will be considered as the scattering objects. These studies performed by scanning electron microscopy showed that several types of defects can be present, the most common one being a half-strength twist disclination loop. These loops lie in the shearing plane (x_1, x_3), and they have a complex structure.[25] We will simplify the real structure by considering the object shown in Figure 7a. It bears the main features of the loops found for thermotropics, i.e. lying in the shearing plane, with the director at a certain angle about the loop main axis (x_3), which varies between the x_3 and the x_2 axes with a helical structure.

In this case, the orientation of the optical axis **d** is characterized by two angles representing the tilt and rotation around the core axis β and ω, respectively (see Figure 7b). In the case of a helical structure, the angle

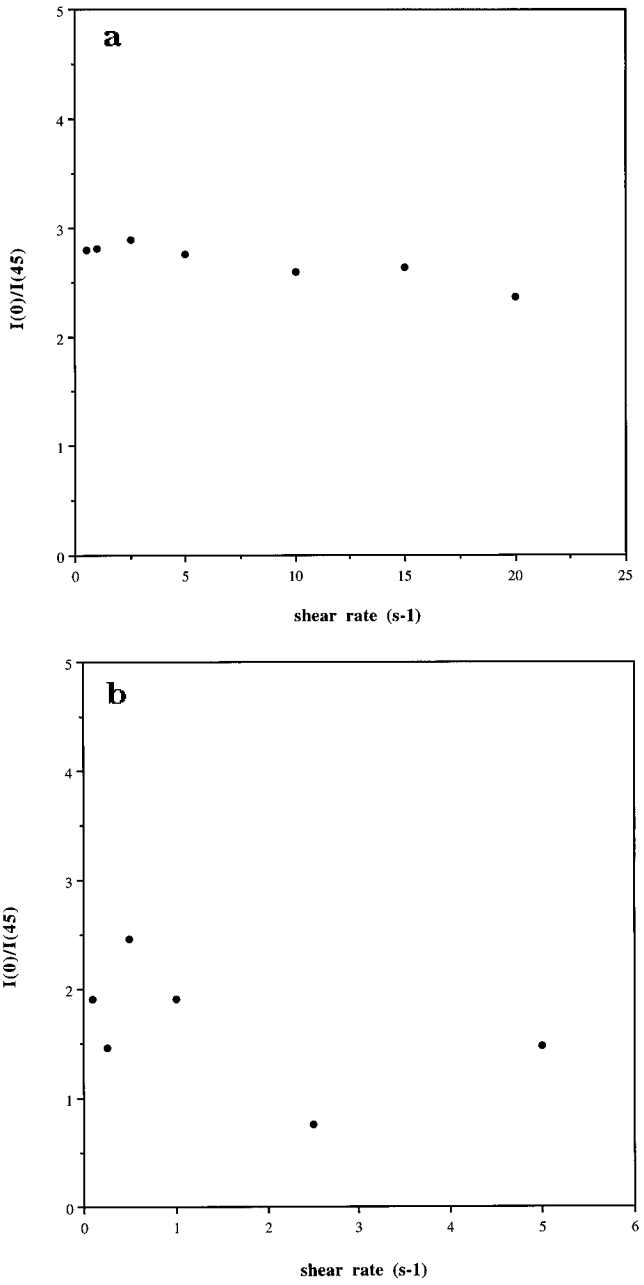

Figure 6. Evolution of the reduced intensity $I(0)/I(45°)$ at $\mu = 90°$ and $\theta = 2.8-3.2°$ as a function of the shear rate: (a) PBG 25%-*m*-cresol 75% solution; (b) HPC L 50%−water 50%.

of rotation is a function of the coordinate along the core, i.e. $\omega = \omega(x_3)$. We shall consider here the simplest linear dependence:

$$\omega(x_3) = 2\pi p x_3 \tag{4.1}$$

where p is the number of rotations per unit of length. For example, for $px_3 = 1$ there is only one turn along the core axis.

A further simplification is introduced by considering only the parts of the loops which are oriented along the flow direction. This means that the model will transform the loop into a set of two rigid rods. A rapid qualitative analysis shows that such a model is in agreement with the experiments described in the previous section since it predicts an intensity maximum at an azimuthal angle of 90°. Light scattering patterns at $\dot{\gamma} \geq \dot{\gamma}_c$ and with HV, VV, and HH polarization positions have an important common feature, i.e. a

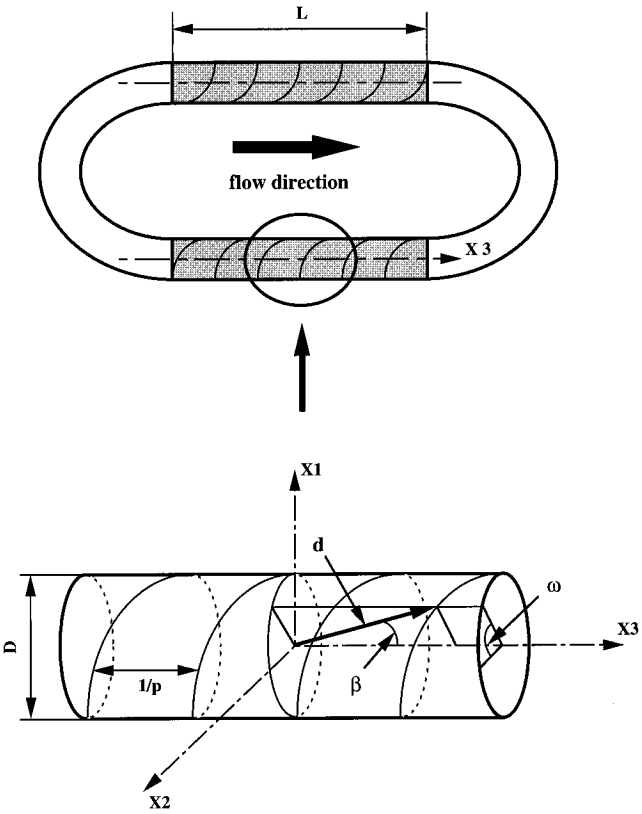

Figure 7. Schematic representation of the defect used for the modeling: (a) the whole loop disclination with the horizontal and vertical parts; (b) detail of the horizontal part; (**d**) director; (β) the tilt angle of the director; (ω) rotation of the director around the core of the defect; (x_1) gradient direction; (x_2) vorticity axis; (x_3) flow direction.

vertical streak which is perpendicular to the direction of flow (see Figure 3). This is compatible with the existence of anisotropic defects stretched along the flow direction. Simultaneous observation of the vertical streak for all positions of polarizers also suggests that the optical axis of the scattering elements has a tilt relative to their main axes. The main contribution to the light scattering along the vorticity axis can be due only to parts of the loops which have a non-zero projection on the x_3 axis. As will be seen later, such a model clearly predicts the behavior of the vertical streak which is due to the horizontal part of the disclination loops, oriented along the flow direction x_3.

The lateral four lobes of the HV patterns must have another physical origin since their dynamics is different from that of the vertical streak. Other parts of the disclination loops, having a projection on the x_1 axis, must be responsible for the lobes. As a preliminary hypothesis we suggest that the following mechanism may occur: The vertical parts of the disclination loops can be considered as obstacles which produce hydrodynamic perturbation of stream lines in the (x_2, x_3) plane. This will induce a rearrangement of the surrounding director in accordance with the nonhomogeneous strain and stress distribution in the vicinity of these parts of disclinations and will contribute to an additional local polarizability field which can be a source of additional light scattering. A theoretical analysis of a similar effect has been performed recently by considering the perturbation of isotropic polymer suspensions due to the presence of solid particles which also predicted a four-leaf HV scattering pattern.[33] The behavior of flowing nematic LCP's is much more complicated than isotropic liquids, but the physical natures of the perturbations of the stream lines in both cases may be similar. The optical observation of a four-leaf pattern around a large rigid obstacle placed in a flowing liquid crystalline polymer solution[34] is predicted by such a hypothesis.

5. Theory

We will study the light scattering from the horizontal parts of the disclination loops of Figure 7 which are oriented parallel to the flow direction. First, we will consider the light scattered by a single rod with a spiral-like orientation of the optical axis. We will then study the 3D diffraction of a set of such anisotropic rods in order to take into account the experimental oscillation of the scattering intensity in the vertical streak.

5.1. Light Scattering by a Single Rod with a Helical Orientation of the Optical Axis. Let us consider a straight cylindrical rod with a diameter of D and a length L, oriented along the x_3 axis (see Figure 7b). The unit vector **d** of the optical axis has a random tilt β around the rod axis which can fluctuate around an average value with a Gaussian distribution function:

$$P(\beta) = c' \exp\left\{\frac{(\beta - \bar{\beta})^2}{2\sigma_\beta^{\,2}}\right\} \qquad (5.1)$$

where σ_β is the dispersion of the angle β and c' is a normalizing coefficient. Vector **d** is rotating around the rod axis in accordance with eq 4.1 and can be written as

$$\mathbf{d} = \mathbf{i} \sin\beta \sin\omega + \mathbf{j} \sin\beta \cos\omega + \mathbf{k} \cos\beta \qquad (5.2)$$

where **i**, **j**, and **k** are the unit vectors along the x_1, x_2, and x_3 axes of the laboratory coordinate system.

In the general case of anisotropic media, the dipole moment induced in a rod by the incident light will depend on the effective orientation of the optical axes, determined by the position of the crystallographical axes of both medium and rod, as well as their polarizabilities. Such a calculation is very complex. In addition, these characteristics are not known. For these reasons, the surrounding medium is considered as being isotropic. This simplification keeps anyhow the main physical features of the problem. The dipole moment induced in the rod by an incident wave with an electric strength E_0 is[35]

$$\mathbf{M} = E_0[\delta(\mathbf{ed})\mathbf{d} + b_t\mathbf{e}] \qquad (5.3)$$

where $\delta = \alpha_1 - \alpha_t$ and $b_t = \alpha_t - \alpha_s$; α_1, α_t, and α_s are the polarizabilities along and across the rod and of the surrounding medium, respectively. The unit vector **e** is parallel to the transmission direction of the polarizer which is in the (x_2, x_3) plane. If the polarizer is tilted by an angle ψ relative to the x_3 axis, then

$$\mathbf{e} = \mathbf{j} \sin\psi + \mathbf{k} \cos\psi \qquad (5.4)$$

The amplitude of the light scattering is expressed as

$$f = C\int_v (\mathbf{MO}) \exp[-i(\mathbf{qr})]\, d^3r \qquad (5.5)$$

where $\mathbf{q} = q\mathbf{s} = q(\mathbf{s}_0 - \mathbf{s}')$ is the scattering vector. Its value depends on the wavelength λ in the medium and the scattering angle θ: $q = (4\pi/\lambda)\sin(\theta/2)$. The unit vector **s** is parallel to the difference between the wave vectors of the incident and scattered light. Taking into account that the incident beam is directed along the x_1

axis, we find

$$\mathbf{s} = -\mathbf{i}\sin\frac{\theta}{2} + \mathbf{j}\cos\frac{\theta}{2}\sin\mu + \mathbf{k}\cos\frac{\theta}{2}\cos\mu \qquad (5.6)$$

The unit vector **O** in eq 5.5 defines the direction of the electric vector passing through the analyzer.

In the following, we will only consider the crossed position of polarizer and analyzer. For small scattering angles and an arbitrary position of the crossed polarizers, the vector **O** can be given in the following approximate form:

$$\mathbf{O} = \mathbf{j}\cos\psi - \mathbf{k}\sin\psi \qquad (5.7)$$

The scalar product (**MO**) can then be found using eqs 5.2−5.4 and 5.7:

$$(\mathbf{MO}) = \frac{1}{2}E_0\delta\{\sin 2\psi \sin^2\beta\cos^2\omega + \cos 2\psi \sin 2\beta\cos\omega - \sin 2\psi\cos^2\beta\} \qquad (5.8)$$

Substituting eq 5.8 into eq 5.5 and taking into account eq 4.1 for the rotation angle ω around the rod, we can calculate the scattering amplitude f_{HV} at a fixed value of the tilt of the optical axis:

$$f = \frac{1}{2}E_0\delta D^2 LC j_0\left(\frac{1}{2}qDs_1\right)j_0\left(\frac{1}{2}qDs_2\right)A_3(pL,\beta;\psi) \qquad (5.9)$$

where

$$A_3(pL\delta;\psi) = \sin 2\psi \sin^2\beta J_2 + \cos 2\psi \sin 2\beta J_1 - \sin 2\psi\cos^2\beta J_0 \qquad (5.10)$$

and

$$J_0 = j_0(ab)$$

$$J_1 = \frac{1}{2}\{j_0[a(b+1)] + j_0[a(b-1)]\}$$

$$J_2 = \frac{1}{4}\{2j_0(ab) + j_0[a(b+2)] + j_0[a(b-2)]\}$$

$$a = \frac{1}{2}\pi pL \quad \text{and} \quad b = \frac{qs_3}{\pi p} \qquad (5.11)$$

where $j_0(x)$ is the zeroth-order spherical Bessel function of the first kind.

We see that at $\mu = 90°$, the scattering amplitude is a real function. When $\mu = 90°$, the components of the vector **s** of eq 5.6 are

$$s_1 = -\sin\frac{\theta}{2}; \qquad s_2 = \cos\frac{\theta}{2}; \qquad s_3 = 0 \qquad (5.12)$$

Substituting eq 5.12 into eq 5.11, we find

$$J_0 = J_{0,90} = 1; \qquad J_1 = J_{1,90} = j_0\left(\frac{1}{2}\pi pL\right); \qquad J_2 = J_{2,90} = \frac{1}{2}[1 + j_0(\pi pL)] \qquad (5.13)$$

To calculate the scattering intensity from the single rod, we have to take into account the random character of the tilt angle of the optical axis around the rod axis. So, the final expression has to be averaged by the distribution function of eq 5.1:

$$I_1 = \langle f^2\rangle_\beta = \left(\frac{1}{2}E_0\delta D^2 LC\right)^2 {j_0}^2\left(\frac{1}{2}qDs_1\right){J_0}^2\left(\frac{1}{2}qDs_2\right)B_3(pL,\bar{\beta},\sigma_\beta;\psi) \qquad (5.14)$$

where

$$B_3(pL,\bar{\beta},\sigma_\beta;\psi) = \cos^2 2\psi\langle\sin^2 2\beta\rangle {J_{1,90}}^2 + \sin^2 2\psi\langle(\cos^2\beta - \sin^2\beta J_{2,90})^2\rangle \qquad (5.15)$$

In eq 5.14, $\langle ...\rangle_\beta$ implies averaging over β:

$$\langle f^2\rangle = \int_0^{2\pi} f^2(\beta)\, P(\beta)\, d\beta \qquad (5.16)$$

It is important to note that the scattering intensity depends only on the product of the helical structure parameter p and the length L of a rod at an azimuthal angle of 90°. If the rod has no helical structure ($p = 0$) it follows from eq 5.13 that

$$J_{0,90} = J_{1,90} = J_{2,90} = 1$$

$$B_3(pL,\bar{\beta},\sigma_\beta;\psi) = \cos^2 2\psi\langle\sin^2 2\beta\rangle + \sin^2 2\psi\langle\cos^2 2\beta\rangle \qquad (5.17)$$

5.2. Light Diffraction from a Set of Disclination Loops. As mentioned in the Experimental Part, the distribution of the scattered light intensity in the vertical streak is very heterogeneous. It is characterized by a strong oscillation of the intensity as a function of the scattering angle. This behavior can be understood only if diffraction between disclination loops is taken into account. The influence of diffraction effects on a light scattering pattern have been considered before for thin polymer films containing two-dimensional assemblies of anisotropic rods.[37] In our case, a 2D distribution is not enough because of the large thickness of the material in the transparent rheometer (about 400 μm) compared to the size of the individual defects. Loops are located at different levels and can contribute to the diffraction pattern due to the path difference between light beams scattered from different depths. Moreover, each disclination loop is nearly parallel to the shear plane[24,25] and therefore the two horizontal parts have different coordinates along the incident light beam. This can also give rise to diffraction effects. So, we must assume that the nonhomogeneous distribution of scattered light in the vertical streak is due to a 3D diffraction phenomenon.

To study this, we will consider the simplest case: N disclination loops of equal lengths and similar internal core structure will be considered as assembled into one set. The upper and lower horizontal parts of the loops will be regarded as rods which are located in different planes parallel to the screen in this set (Figure 1). The projection of this set onto the (x_1, x_2) plane formed by the incident beam and vorticity axis is shown in Figure 8. The distances l and h between the nearest points of the rods along x_2 and x_3, and the angle α are independent random values obeying Gaussian distributions:

$$P(\xi) = \frac{1}{\sigma_\xi\sqrt{2\pi}}\exp\left\{\frac{(\xi - \bar{\xi})^2}{2{\sigma_\xi}^2}\right\} \qquad (5.18)$$

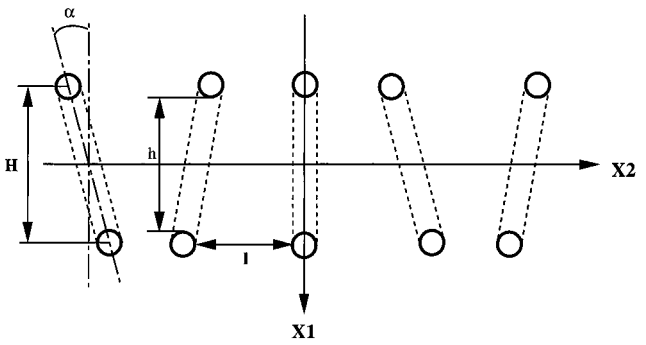

Figure 8. Projection of the disclination loops on the shear rate gradient axis−vorticity axis plane: (x_1) gradient direction; (x_2) vorticity axis; (x_3) flow direction.

where $\bar{\xi}$ is $\bar{h}$, $\bar{\alpha}$, or $\bar{l}$, the average values of h, α, and l; σ_ξ is σ_h, σ_α, or σ_l which are their dispersions.

We will assume that there is no disorder in the orientation of optical axes of the rods in the set. In this case the light scattering intensity from the set under consideration with $2N$ horizontal rods can be written in the following general form:

$$I = I_1\{2N + \langle \sum_{i \neq j}^{2N} \exp[-i\mathbf{q}(\mathbf{r}_i - \mathbf{r}_j)]\rangle_{l,h,\alpha}\} \quad (5.19)$$

where $\mathbf{r}_i - \mathbf{r}_j$ is a vector connecting the centers of the ith and jth rods and the angular brackets, $\langle ... \rangle_{l,h,\alpha}$, represent the averaging over the random values of l, h, and α.

By performing the summation in eq 5.19 for the arrangement of the rods shown in Figure 8, one can show that the following expression for the sum holds:

$$\langle \sum_{i \neq j}^{2N} \exp[-i\mathbf{q}(\mathbf{r}_i - \mathbf{r}_j)]\rangle_{l,h,\alpha} = 2\{\langle[\cos(qs_1H) \times \cos(qs_2H \tan\alpha) + 2]\rangle_{h,\alpha}\langle \sum_{m=1}^{N} m \cos(qs_2((N-m)D + l_1 + ... + l_{N-m}))\rangle_l - 2N\} \quad (5.20)$$

where $H = D + h$ is the distance between the rods in the two depth levels of the set and l_1, l_2, ..., l_n are the distances between different neighboring rods. If we assume that there is no correlation between the position of the rods in the (x_2, x_3) plane, we can average over the values l_n separately. Using eqs 5.14, 5.19, and 5.20, we obtain the light scattering intensity per rod volume in the vertical streak ($\mu = 90°$) from the set of rods:

$$I_{2N} = \frac{I_1}{LD^2}\left\{\frac{1}{N}[\langle\cos(qs_1H)\cos(qs_2H\tan\alpha)\rangle_{h,\alpha} + 2]\sum_{m=1}^{N} m \exp\left[-\frac{1}{2}(N-m)q^2{s_2}^2{\sigma_1}^2\right] \times \cos((N-m)qs_2(D+\bar{l})) - 1\right\} \quad (5.21)$$

The sum in eq 5.21 represents the diffraction effects between rods from one of the planes parallel to the screen. The factor in the square brackets is due to the path difference between the waves scattered by rods lying at different depths in the sample. This factor is also an oscillating function of θ and can strongly modulate the contribution from the sum.

6. Discussion

The theory given in the preceding part has a very general character. Varying the geometrical parameters of the scattering objects (internal structure of the rod, number of rods, number of packs, relative position and dispersion of rods in packs, etc.) can give many different scattering patterns for which trends relating scattering intensity and morphology can be deduced. Such a complete study, interesting in itself, was not performed here. The purpose of the present study is to understand the nature of the defects created during the shear flow of liquid crystalline polymers. Thus we will select, on a best guess basis, a range of "adjustable parameters" which have a physical meaning. We will then vary these parameters in order to fit experiments and theory.

6.1. Comparison between Theory and Experimental Observations. The theory shows that if we consider either a single rod (with the rod geometry given in Figure 7) or a set of aligned rods, the scattering patterns are characterized by a very strong intensity maximum around an azimuthal angle of ±90°, similar to the vertical streak found experimentally (there are of course several polarizer positions with selected director arrangements for which there is no scattering). This result was expected since we are dealing with aligned rods.

In no case could a pattern with four lobes in HV polarization be predicted. This provides the first result: The four lobes found experimentally cannot be explained with this model. This is consistent with the experimental observation that the vertical streak and the four lobes have different relaxation behaviors, an indication that they are caused by different physical mechanisms.

The theory shows that the intensity of the light scattered at $\mu = \pm 90°$ as a function of the scattering angle θ depends very strongly on the set of structural parameters describing the rods which are chosen. We can separate the following parameters.

(i) The parameters describing the rod itself. The internal structure will be studied at a fixed scattering angle (in practice we considered a small scattering angle range of 2.8−3.2° to increase the signal to noise ratio) by analyzing the dependence of the reduced intensity $I(\psi)/I(45)$ on the angle ψ (the angle between the crossed polarizers and the flow direction).

(ii) The parameters describing the inter-rod arrangement. At a fixed value of ψ, the qualitative behavior of the reduced intensity $I(\psi)/I(45)$ versus scattering angle θ does not depend on the value of the internal structure parameters.

This can be seen by examining eqs 5.14 and 5.21. They show that the dependence of the scattered intensity (at $\mu = 90°$) is determined by the diameter of the rod, D, and the parameters describing the set of rods (number of rods, $2N$; average distances $\bar{l}$ and $\bar{h}$; dispersions σ_l and σ_h; angle of deviation from the shear plane α; and its dispersion σ_α). The internal structure of the rod is characterized by three parameters, pL, $\bar{\beta}$, and σ_β which are included in the prefactor B_3 (eq 5.15). This allows us to perform and experimentally test a decoupling between the internal structure of the rod and the inter-rod arrangement.

6.2. Inter-rod Arrangement. Selection of Parameters and Exploitation of the Curves. A first

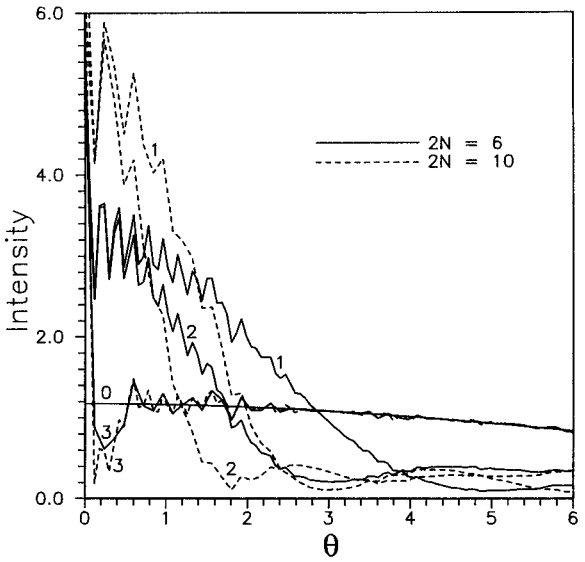

Figure 9. Prediction of the scattered intensity at $\mu = 90°$ as a function of the scattering angle θ for different numbers of assembled loops and average distances l between the rods. $D = 31$, $\sigma_\beta = 0.1$, $p = 0$, $h = 100D$. Key: (0) single rod; (1) $l = 0.3D$; (2) $l =$ D; (3) $l = 25D$.

guess, based on microscopy observations and "reasonable" estimates, gives the following values for the parameters: $D = 3\lambda$, $\bar{\beta} = 60°$, and $\sigma_\beta = 0.2$. $D = 3\lambda$ is based on optical microscopy for thermotropic polymers.[25] The angle β must be larger than 45° because the intensity of the vertical streak in the HH position is larger than that in the VV position. The dispersion σ_β is more difficult to estimate, and its value was chosen after some numerical tests, in order to match the experimental curves. Three different averaged distances between rods in the (x_2-x_3) plane were chosen, $\bar{l} = kD$, with $k = 0.1$, 1, and 25. They correspond to very close, intermediate, and loose packings. The distance between the nearest rods at different depth levels along the incident light direction was fixed rather arbitrarily at $\bar{h} = 100D$, with $\sigma_h = 0$. In order to get an intensity versus scattering curve matching the experiments, the fluctuation of the plane of "loops", i.e. of two rods belonging to two different depth levels, was chosen to depend on the averaged distance $\bar{l}$, $\sigma_l = 0.4\bar{l}$. An increase of $\bar{l}$ was supposed to induce an increase of the width of the distribution function $P(l)$ (see eq 5.18). This makes sense since an increase of interaction between rods will induce a better determined relative position of the loops.

The scattering intensity (in arbitrary units) is calculated with the above parameters for two different numbers of rods ($2N = 6$ and $2N = 10$) inside each set and is shown in Figure 9. The qualitative behavior of the curve is very similar to the experimental intensity given in Figure 3, with an oscillating decrease of the intensity with scattering angles. Figure 9 shows that the calculated scattering curves are characterized by large oscillations of intensity at small scattering angles. This is caused by the light diffraction from the rods being at a different depth. At the same time we can see that the behavior of the scattering intensity is different for sets with different numbers of rods $2N$ and/or distances $\bar{l}$ between them. Figure 9 demonstrates that an increase of N gives an increase of the intensity and amplitude of the oscillations. It gives also a sharper reduction of the intensity with increasing scattering angle θ.

We will now observe that quantitative relative information on the arrangement between rods can be obtained from the scattering curves. First, eq 5.20 shows that the ratio of the intensity maxima for two different sets noted 1 and 2 at very small values of θ is equal to the ratio of the number of rods in these sets, i.e. $I_1^{max}/I_2^{max} \approx N_1/N_2$, and does not depend on the distance between rods $\bar{l}$ and dispersion σ_l. The decrease of $\bar{l}$ and/or σ_l makes only the scattering curves broader (see Figure 9). Second, the ratio θ_1/θ_2 of scattering angles corresponding to the first deep minimum of the calculated intensities for two different sets 1 and 2 with numbers of rods N_1 and N_2, keeping the same distance between rods ($\bar{l}_1$ $\bar{l}_2$, $\sigma_{l_1} = \sigma_{l_2}$), is inversely proportional to the number of rods, i.e. $\theta_1/\theta_2 \approx N_2/N_1$. If $\bar{l}_1 > \bar{l}_2$ or $(\sigma_{l_1} > \sigma_{l_2})$, we have $\theta_1/\theta_2 < N_2/N_1$. The precise location of this first deep minimum is difficult to find on the experimental curves. The same relation between θ and N can be approximately found if we use for the scattering angle the one obtained at the cross-section of the θ axis and the scattering intensity curve averaged over a small region of θ, before the first minimum.

Comparison with Experiments. Experimental scattering curves show a change of the magnitude of both *mean intensity* and *oscillations* at small scattering angles with increasing shear rate for both HPC and PBG solutions (ref 26). Figure 3 gives an example of $I_{\mu=90°}$ at two different shear rates for the PBG solution. The same tendency is shown in Figure 9 when the number of rods in sets increases.

For the PBG solution the average ratio between intensity maxima for $\dot{\gamma} = 15$ and 0.5 s^{-1} at $\theta = 0.5°$ is equal to 2. It means that there are 2 more rods per set at $\dot{\gamma} = 15$ s^{-1} than at $\dot{\gamma} = 0.5$ s^{-1}. We can also consider the ratio of scattering angles defined above. For the same two values of shear rate (0.5 and 15 s^{-1}), we have $\theta_{0.5}/\theta_{15} \approx 1.5$ for PBG. According to the previous discussion, it means that the number of rods is larger by a factor of 1.5 at 15 s^{-1}, close to the factor 2 found by analyzing the behavior of the intensity maxima. This shows the consistency of this analysis.

6.3. Internal Structure of Defects. To study the internal structure of the scattering elements, we have to exclude the parameters linked to their arrangement in sets. According to the theory, we can do it by reducing the scattering intensity to its value at $\psi = 45°$. As a result, we obtain from eqs 5.14 and 5.20 the following function:

$$R = \frac{I}{I(45)} = \frac{B_3(pL,\bar{\beta},\sigma_\beta,\psi)}{B_3(pL,\bar{\beta},\sigma_\beta,45)} \qquad (6.1)$$

which depends only on the parameters associated with the rod and the angle ψ describing the position of the crossed polarizers.

The calculated dependence of R on ψ is shown on Figure 10. The curves are symmetrical relative to $\psi = 45°$ and characterized by maxima and minima depending on the product pL. A symmetry of R around $\psi = 45°$ is possible only for a parallel orientation of the optical axis of the rods in sets.

The measured reduced intensity for the PBG and the HPC solutions are given in Figures 4 and 5. PBG and HPC have similar behaviors, a nearly symmetrical decrease and increase of intensity around $\psi = 45°$. This is very similar to what is theoretically given in Figure 11. The fact that the experimental curves are symmetrical suggests that the loops belonging to the same

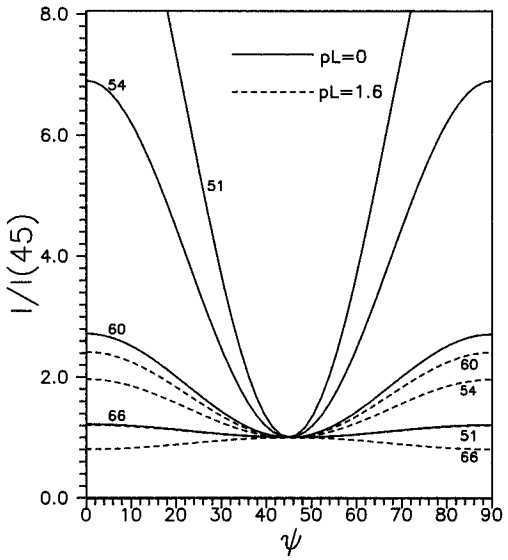

Figure 10. Prediction of the reduced scattered intensity $I/I(45°)$ at $\mu = 90°$ and $\theta = 3°$ as a function of the position of the crossed polarizers for different values of the tilt and the spiral parameter pL. $\sigma_\beta = 0.1$.

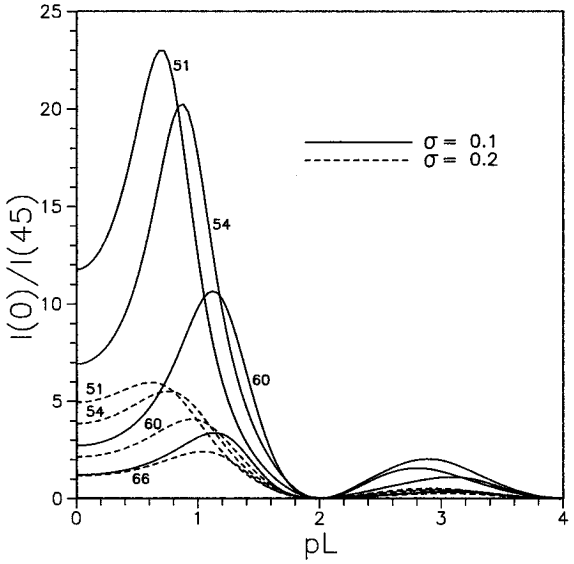

Figure 11. Prediction of the reduced scattered intensity $I/I(45°)$ at $\mu = 90°$ and $\theta = 3°$ as a function of the spiral parameter pL for different values of the average tilt β and the dispersion σ_β.

set have a strong orientation correlation for both polymers. We can now compare more closely Figures 4 and 5 and Figure 11.

Figure 11 shows that the reduced intensity is very sensitive to the values of the average tilt $\bar{\beta}$ and to the parameter pL. We can see that for $p = 0$ the curve becomes flatter when $\bar{\beta}$ increases.

Figures 11 and 12 show the dependence of $R(0) = I(0)/I(45)$ on pL and σ_β. We can see from Figure 11 that the appearance of a helical structure induces a nonmonotonic behavior of $R(0)$ with increasing pL. The magnitude and position of the maxima depend on $\bar{\beta}$ and σ_β. At a fixed value of the dispersion, the maximum is growing and displaced in the direction of small values of pL with decreasing $\bar{\beta}$. An increase of the dispersion decreases $R(0)$. Figure 12 shows that this change is monotonic. $R(0)$ is smaller than unity at large values of the dispersion σ_β. The experimental intensity reduced to $I(45)$ is shown in Figures 5 and 6. Let us consider

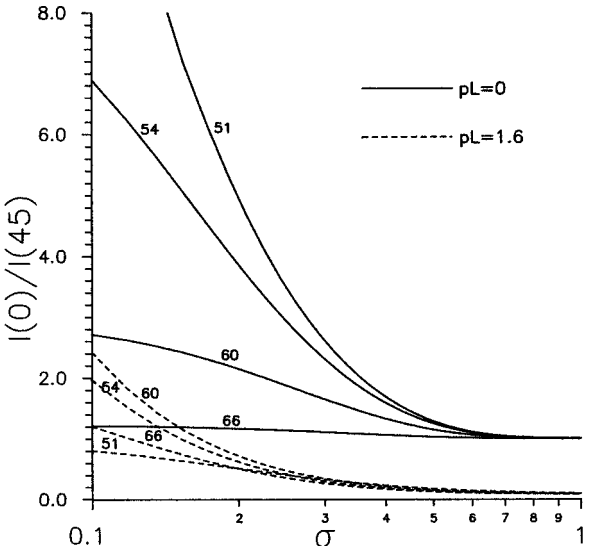

Figure 12. Prediction of the reduced scattered intensity $I/I(45°)$ at $\mu = 90°$ and $\theta = 3°$ as a function of the dispersion σ_β for different values of the average tilt β and the spiral parameter pL.

the behavior of $R(0)$ as a function of the shear rate for PBG and HPC solutions.

Figure 6a shows that $R(0)$ for PBG is approximately constant and equal to ≈3, in a broad range of shear rates, from 0.5 to 20 s^{-1}. According to the above theoretical analysis (see Figure 12) this value can be obtained for $p = 0$ and $\bar{\beta}$ close to 60°, with a very precise orientation of the optical axis, $\sigma_\beta < 0.1$ A helical structure at $\bar{\beta} \geq 60°$ will strongly increase the value of $R(0)$ above 3 for values of pL larger than 0.4. It is not in agreement with the experiments. We can thus conclude that the orientation of the optical axis of the disclination cores in PBG solution does not depend on the shear rate in the range 0.5−20 s^{-1} and has a precisely fixed angle $\bar{\beta} = 60°$. There is no or a weak helical orientation of the director around the core.

The behavior of the reduced intensity for HPC solution at shear rates in the range 0.1−5 s^{-1} is completely different. We can see from Figure 5 that an increase of the shear rate induces a change of the shape of the curves. The value $R(0)$ is changing around 1.2−2.5 s^{-1}. The lowest value of $R(0)$ is for the highest shear rate ($\dot{\gamma} = 5$ s^{-1}). The dependence of $R(0)$ for the HPC solution on shear rate is shown in Figure 6b. The analysis of Figures 11 and 12 shows that in order for $R(0)$ to be in the range 1−2.5, we have to take $\bar{\beta}$ around 60°, but with a large dispersion (σ_β about 0.2). In this case, Figure 11 shows a small maximum for pL and then a slow decrease with increasing pL. This is similar to the experimental shape of $R(0)$ versus shear rate (see Figure 6b). One possibility for explaining these data is to consider a helical orientation of the director around the rod axis. An increase of the shear rate increases pL from 0 at small $\dot{\gamma}$ to 1.2 at $\dot{\gamma} = 5$ s^{-1}. It means that there is about one full turn of the director per length of rod at high shear rates.

7. Conclusions

The light scattering behavior of polymer liquid crystals is very rich and without doubt very instructive if one hopes to understand the rheology of this class of materials. The present work is one of the first attempts to model and interpret SALS during shear. Only one single feature of the SALS patterns (the vertical streak)

obtained in one given steady state shear rate range was analyzed. This is not much owing to the large variety of flow behaviors displayed by such materials, but even this limited task turned out to be very complicated. It required the previous knowledge of the kind of supermolecular structure created during flow for deriving a tractable model. The interesting point is that this model and its associated light scattering prove to be able to reproduce the experimental data. As usual, it points out the weakness of light scattering experiments (you must know the structure that is responsible for the scattering in advance) and the power of this technique since it is possible to measure (or evaluate) structural parameters by comparing experiments and theory.

In the present case of LCP, the following structural features were found.

(i) In the intermediate shear rate range where dark lines are seen by optical microscopy, mainly at low shear rates before the occurrence of the second positive zone of the first normal stress difference, in a region where tumbling is thought to occur, SALS results confirm that the disclination loops found previously in one thermotropic polymer can produce light scattering features that are seen with two lyotropic LCP's.

(ii) According to the SALS, the disclination loops are assembled into sets. For PBG solutions, the number of loops per set is increasing in the flow regime described above.

(iii) The orientation of the optical axis in the core of the disclination does not change when changing the shear rate for PBG and has a value close to 60° about the core axis (the flow direction). There is no or a weak helical winding up of the director around the core axis. The situation for HPC is different since there is a helical winding up of the director around the core axis, changing with the shear rate.

Acknowledgment. This work has been supported by the Direction des Recherches, Etudes et Techniques du Ministère de la Défense, and by the Commission of the European Community (Brite Euram program).

Notation

D	diameter of the rod (theory)
d	unit vector of the optical axis
e	unit vector parallel to the transmission direction of the polarizer which is in the (x_2, x_3) plane
h	inter-rod distance (Figure 8)
HV	crossed polarization, with the H polarization direction defined as being along the flow direction
i, **j**, and **k**	the unit vectors along the x_1, x_2, and x_3 axes of the laboratory coordinate system
L	length of the rod
l	inter-rod distance (Figure 8)
M	induced dipole moment
N	number of loops in one set ($2N$ represents the number of rods in the set)
O	unit vector defining the direction of the electric vector passing through the analyzer
p	number of rotations per unit of length
s	unit vector (eq 4.5)
x_1, x_2, and	gradient direction, vorticity axis, and flow direction
α x_3	angle defined in Figure 9
α_i	polarizabilities of the rod
β	tilt angle around the rod axis
θ (or **q**)	polar scattering angle (or scattering vector **q** with $q = (4\pi/\lambda)\sin(\theta/2)$)
μ	azimuthal scattering angle
ψ	direction of the optical axis of the polarizer according to the flow direction
$\dot{\gamma}$	shear rate
ω	rotation angle around the core axis
σ_x	dispersion of the parameter x

References and Notes

(1) Doi, M. *J. Polym. Sci., Polym. Phys. Ed.* **1981**, *19*, 229.
(2) Marrucci, G.; Maffetone, P. L. *Macromolecules* **1989**, *22*, 4076.
(3) Larson, R. G.; Öttinger, H. C. *Macromolecules* **1991**, *24*, 6270.
(4) Marrucci, G.; Greco, F. *J. Non-Newtonian Fluid Mech.* **1992**, *44*, 1.
(5) Larson, R. G.; Doi, M. *J. Rheol.* **1991**, *35*, 539.
(6) Hongladarom, K.; Burghardt, W. R.; Baek, S. G.; Cementwala, S.; Magda, J. J. *Macromolecules* **1993**, *26*, 772.
(7) Hongladarom, K.; Burghardt, W. R. *Macromolecules* **1993**, *26*, 785.
(8) Kiss, G.; Porter, R. S. *J. Polym. Sci., Polym. Symp.* **1978**, *65*, 193.
(9) Jerman, R. E.; Baird, D. H. *J. Rheol.* **1981**, *25*, 275.
(10) Moldenaers, P.; Mewis, J. *J. Rheol.* **1986**, *30*, 567.
(11) Coccini, F.; Nobile, M. R.; Acierno, D. *J. Rheol.* **1991**, *35*, 1171.
(12) Magda, J. J.; Baek, S. G.; de Vries, K. L.; Larson, R. G. *Macromolecules* **1992**, *24*, 4460.
(13) Kiss, G.; Porter, R. S. *Mol. Cryst. Liq. Cryst.* **1980**, *60*, 267.
(14) Asada, T.; Toda, K.; Onogi, S. *Mol. Cryst. Liq. Cryst.* **1981**, *68*, 231.
(15) Moldenaers, P.; Fuller, G.; Mewis, J. *Macromolecules* **1989**, *22*, 960.
(16) Ernst, B.; Navard, P.; Hashimoto, T.; Takebe, T. *Macromolecules* **1990**, *23*, 1370.
(17) Hsiao, B. S.; Stein, R. S.; Deutscher, K.; Winter, H. H. *J. Polym. Sci., Polym. Phys. Ed.* **1990**, *28*, 1571.
(18) Picken, S. J.; Aerts, J.; Doppert, H. L.; Reuvers, A. J.; Northold, M. G. *Macromolecules* **1991**, *24*, 1366.
(19) Keates, P.; Mitchell, G. R.; Peuvrel-Disdier, E.; Navard, P. *Polymer* **1993**, *34*, 141.
(20) Srinivasarao, M.; Berry, G. C. *J. Rheol.* **1991**, *35* (3), 379.
(21) Burghardt, W. R.; Fuller, G. G. *Macromolecules* **1991**, *24*, 2546.
(22) Graziano, D. J.; Mackley, M. R. *Mol. Cryst. Liq. Cryst.* **1984**, *106*, 73.
(23) Takebe, T.; Hashimoto, T.; Ernst, B.; Navard, P.; Stein, R. *J. Chem. Phys.* **1990**, *92*, 1386.
(24) De'Nève, T.; Kléman, M.; Navard, P. *C. R. Acad. Sci., Ser. II* **1993**, *316*, 1037.
(25) De'Nève, T.; Navard, P.; Kléman, M. *Macromolecules* **1995**, *28*, 1541.
(26) Riti, J. B.; Navard, P. *Synth. Polym. J.* **1994**, *1*, 1.
(27) Rojstaczer, S.; Stein, R. S. *Mol. Cryst. Liq. Cryst.* **1988**, *157*, 293.
(28) Shiwaku, T.; Nakai, A.; Hasegawa, H.; Hashimoto, T. *Macromolecules* **1990**, *23*, 1590.
(29) Shukla, P.; Muthukumar, M. *J. Polym. Sci., Polym. Phys. Ed.* **1991**, *29*, 1373.
(30) Greco, F. *Macromolecules* **1989**, *22*, 4622.
(31) Patlazhan, S.; Riti, J. B.; Navard, P. Light Scattering from Lyotropic Textured Liquid-Crystalline Polymers Under Shear Flow. In *Flow-Induced Structures in Polymers*; ACS Symposium Series 597; Nakatani, A. I., Dadmun, M. D., Eds.; American Chemical Society: Washington, DC, 1995; p 298.
(32) Cidade, T.; Riti, J. B.; Navard, P. Manuscript in preparation.
(33) Patlazhan, S.; Navard, P. *J. Phys.* **1995**, *5*, 1.
(34) Peuvrel, E.; Navard, P. *Macromolecules* **1991**, *24*, 5683.
(35) Hashimoto, T.; Ebisu, S.; Inaba, N.; Kawai, H. *Polym. J.* **1981**, *13*, 701.
(36) Stein, R. S.; Wilson, P. R. *J. Appl. Phys.* **1962**, *33*, 1914.
(37) Hashimoto, T.; Ebisu, S.; Kawai, H. *J.* Polym. *Sci., Polym. Phys. Ed.* **1981**, *19*, 59.

MA946435M